JACS
JOURNAL OF THE AMERICAN CHEMICAL SOCIETY
Article
pubs.acs.org/JACS

Interaction of Cisplatin with Adenine and Guanine: A Combined IRMPD, MS/MS, and Theoretical Study

Barbara Chiavarino,*[,†] Maria Elisa Crestoni,[†] Simonetta Fornarini,[†] Debora Scuderi,[‡,§] and Jean-Yves Salpin*[,⊥,∥]

[†]Dipartimento di Chimica e Tecnologie del Farmaco, Università di Roma "La Sapienza", P.le A. Moro 5, I-00185 Roma, Italy

[‡]Laboratoire de Chimie-Physique, Université Paris Sud Orsay, Avenue Georges Clémenceau, 91405 Orsay Cedex, France

[§]CNRS-UMR 8000

[⊥]Université d'Evry Val d'Essonne, Laboratoire Analyse et Modélisation pour la Biologie et l'Environnement, Boulevard François Mitterrand, 91025 Evry, France

[∥]CNRS-UMR 8587

Supporting Information

ABSTRACT: Infrared multiple photon dissociation (IRMPD) spectroscopy of *cis*-$[Pt(NH_3)_2(G)Cl]^+$ and *cis*-$[Pt(NH_3)_2(A)Cl]^+$ ions (where A is adenine and G is guanine) has been performed in two spectral regions, 950−1900 and 2900−3700 cm^{-1}. Quantum chemical calculations at the B3LYP/LACV3P/6-311G** level yield the optimized geometries and IR spectra for the conceivable isomers of *cis*-$[Pt(NH_3)_2(G)Cl]^+$ and *cis*-$[Pt(NH_3)_2(A)Cl]^+$, whereby the cisplatin residue is attached to the N7, N3, or carbonyl oxygen atom, (O6), of guanine and to the N7, N3, or N1 position of adenine, respectively. In addition to the conventional binding sites of native adenine, complexes with N7−H tautomers have also been considered. In agreement with computational results, the IR characterization of *cis*-$[Pt(NH_3)_2(G)Cl]^+$ points to a covalent structure where Pt is bound to the N7 atom of guanine. The characterized conformer has a hydrogen-bonding interaction between a hydrogen atom of one NH_3 ligand and the carbonyl group of guanine. The experimental C═O stretching feature of *cis*-$[Pt(NH_3)_2(G)Cl]^+$ at 1718 cm^{-1}, remarkably red-shifted with respect to an unperturbed C═O stretching mode, is indicative of a lengthened CO bond in guanine, a signature that this group is involved in hydrogen bonding. The IRMPD spectra of *cis*-$[Pt(NH_3)_2(A)Cl]^+$ are consistent with the presence of two major isomers, **PtAN3** and **PtAN1**, where Pt is bound to the N3 and N1 positions of native adenine, respectively.

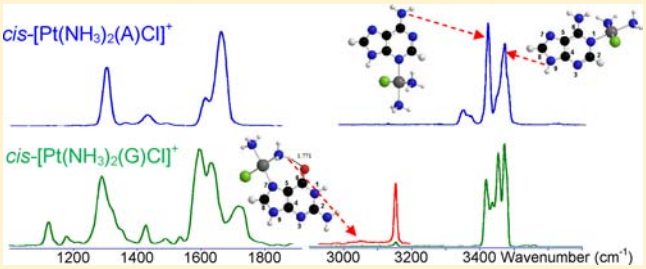

1. INTRODUCTION

cis-Diamminedichloroplatinum(II), commonly known as cisplatin (*cis*-$[Pt(NH_3)_2Cl_2]$), is a widely used anticancer drug that has been particularly successful in treating lung, ovarian, testicular, head, and neck tumors.[1] Since its discovery some 40 years ago,[2,3] many efforts have been devoted to understanding the mechanisms associated with its antitumor activity,[4,5] which are now quite well established. The primary target of cisplatin is genomic DNA, and more specifically the N7 position of guanine bases. Cisplatin enters the cell by passive diffusion through the cell membrane. The biologically active substrate, namely *cis*-$[Pt(NH_3)_2(H_2O)Cl]^+$, is then formed within the cell, a process promoted by the low chloride concentration inside the cell. It interacts with a guanine residue at the N7 position, thereby generating the monofunctional adduct by loss of water. In a subsequent step, the second chlorine atom is expelled, and coordination to the N7 position of an adjacent purine results in what is called an intrastrand cross-link.[6,7] These intrastrand cross-links are mainly 1,2-d(GpG) and to a lesser extent 1,2-d(ApG). 1,2-Intrastrand cross-links structurally distort the DNA duplex[8,9] and ultimately lead to the genotoxicity and antitumor activity.

In spite of the clinical success of cisplatin, side effects and the natural and acquired resistance of patients toward the drug have motivated searches for structurally and/or functionally analogous alternatives. Unfortunately, finding analogous compounds that outperform cisplatin has proved to be difficult. Thousands of platinum compounds have indeed been synthesized during more than four decades. However, only few new agents such as oxaliplatin, carboplatin, and nedaplatin[5] have been registered worldwide and entered clinical practice. Although there is no doubt that a Pt−N7 bond forms during initial attack, the exact structure of the monofunctional adduct is not well known. In this context, a better understanding at the molecular level of the interactions between the Pt and DNA building blocks is expected to be helpful in establishing a new strategy to design cisplatin analogues. Such information may be

Received: October 5, 2012
Published: December 28, 2012

   dx.doi.org/10.1021/ja309857d | J. Am. Chem. Soc. 2013, 135, 1445−1455

accessible through gas-phase studies, and the present paper is the first of a series of articles dealing with the experimental structural characterization of cisplatin/DNA components in the gas phase. We opted for a strategy based upon the gradual increase of the size of the nucleic acid building blocks. We presently report the structural characterization of gas-phase complexes arising from the interaction between cisplatin and the two nucleobases known to be involved in cross-links, namely guanine and adenine.

To perform this study, we combined tandem mass spectrometry (MS/MS) experiments with density functional theory (DFT) calculations, and also recorded the infrared multiple photon dissociation (IRMPD) spectra of the electrospray ionization (ESI)-generated complexes. IRMPD spectroscopy of mass-selected ions is now established as a powerful approach for the structural characterization of gaseous ions[10−15] and notably nucleotides,[16] and has been successfully applied to metal ion/biomolecules systems.[12,17−32] This ion spectroscopy is often termed "action spectroscopy" since resonant IR absorption cannot be directly probed due to the low ion density within mass spectrometers. Nevertheless, through the use of intense IR sources, ion fragmentation can be induced by a multiple photon absorption process. Two distinct energy domains were considered. First, IRMPD spectra were recorded in the 950−1900 cm^{-1} energy region by combining a free electron laser to a Fourier transform ion cyclotron resonance (FT-ICR) instrument. IR spectra in the 2900−3700 cm^{-1} frequency range were also recorded using an optical parametric oscillator (OPO) laser. This spectral range is of particular interest for probing the vibrational shifts associated with the NH and OH stretches involved in hydrogen bonds.

2. EXPERIMENTAL SECTION

2.1. Materials. *cis*-Diamminedichloroplatinum(II) (cisplatin), 2′-deoxyadenosine-5′-monophosphate (5′-dAMP), 2′-deoxyguanosine-5′-monophosphate (5′-dGMP), and water used in this work were research-grade products from commercial sources (Sigma-Aldrich, Milan, Italy) and were used without any further purification. Stock aqueous solutions of cisplatin and of the two deoxynucleotides were prepared at 10^{-3} M concentrations. In order to generate the complexes of interest in the gas phase, deoxynucleotides were used instead of the nucleobases, given the poor solubility of the latter in any solvent. A 10^{-4} M water solution of cisplatin and analyte (5′-dGMP or 5′-dAMP) were mixed together in the molar ratio of 1:1, and the reaction continued at room temperature for 24 h, to allow the formation of the different complexes before the analysis. In order to obtain the mixed complex $[Pt(A)(G)(-H)]^+$ (where A is adenine and G is guanine), an aqueous solution with final concentration of 10^{-4} M was prepared by mixing the three stock solutions of cisplatin, 5′-dGMP, and 5′-dAMP in the molar ratio 1:1:1 and allowing them to react for at least 20 days at room temperature prior to analysis.

2.2. CID and IRMPD Experiments. Gaseous ions were generated using an ESI source through direct infusion by a syringe pump. Collision-induced dissociation (CID) experiments at variable energy were carried out using an Applied Biosystems 2000 Q-Trap instrument, a commercial hybrid triple-quadrupole linear ion trap mass spectrometer ($Q1q2Q_{LIT}$). Typical ESI conditions were a flow rate of 10 μL/min, a declustering potential set to 90 V, and an entrance potential of 8 V. The ion of interest was mass-selected using Q1. CID experiments were performed in the quadrupole collision cell q2 at variable collision energies (E_{lab} = 5−50 eV) with N_2 as collision gas at a nominal pressure of 3.3×10^{-5} mbar. The dissociation product pattern was monitored by scanning Q_{LIT} using the enhanced mode of operation where the ions, formed in collision cell q2, are trapped in Q_{Lit} for 10 accumulation spectra in order to increase both the resolution and intensity. A certain extent of fragmentation products, which did not appreciably change in the early steps of increasing E_{lab}, was observed even at the lowest E_{lab} value of 5 eV that was allowed by the instrumental parameters. This early dissociation is ascribed to the presence of collision gas not only in q2 but also in the region between Q1 and q2.[33−35] This explanation is supported by the pressure dependence of the relative fraction of these products. Quantitative threshold information is not directly available.[27,33,36,37] However, for a comparative analysis of the energy-dependent CID experiments, the collision energies were converted to the center-of-mass frame $E_{CM} = [m/(m + M)]E_{lab}$, in which m and M are the masses of the collision gas and of the ion, respectively. Relative abundances of fragment ions display an energy dependence that can be modeled by a sigmoid function, and phenomenological appearance energies may be derived from linear extrapolation of the rise of the sigmoid curves to the baseline.[33,38,39]

IRMPD experiments on *cis*-$[Pt(NH_3)_2(A)Cl]^+$ and *cis*-$[Pt(NH_3)_2(G)Cl]^+$ ions were performed in two spectral regions, 950−1900 and 2900−3700 cm^{-1}, using two different IR radiation sources, the free electron laser (FEL) at the Centre Laser Infrarouge d'Orsay (CLIO) facility and an optical parametric oscillator/amplifier (OPO/OPA) laser system at the Università di Roma "La Sapienza", respectively. The FEL radiation is generated by a 10−50 MeV electron linear accelerator and is delivered in 8-μs-long macropulses at a repetition rate of 25 Hz, each containing a few hundred micropulses (a few picoseconds long). Typical macropulse energies are 40 mJ. Ions were irradiated for 250 ms to 1 s with the IR FEL radiation. For the present study, the FEL was operated at 45 MeV in order to optimize the laser power in the frequency region of interest. The laser wavelength profile was monitored at each reading with a monochromator associated with a pyroelectric detector array (spiricon).

FEL-based experiments were performed using an APEX-Qe Bruker hybrid FT-ICR tandem mass spectrometer equipped with a 7.0 T actively shielded superconducting magnet and a quadrupole−hexapole interface for mass-filtering and ion accumulation, under control by the commercial software APEX 1.0. This particular experimental setup has already been described in detail elsewhere.[40] *cis*-$[Pt(NH_3)_2(A)Cl]^+$ and *cis*-$[Pt(NH_3)_2(G)Cl]^+$ ions were mass-selected in the quadrupole and accumulated in a hexapole containing argon buffer gas for 0.5 s for collisional cooling. Ions were then pulse-extracted toward the ICR cell, where mass-selection of the complexes was performed. They were then irradiated with IR light, after which the resulting ions were mass-analyzed.

A LaserVision OPO/OPA coupled to a Paul ion trap tandem mass spectrometer (Esquire 6000+, Bruker Inc.) was employed to explore the 2900−3700 cm^{-1} spectral region of the different species under study. This parametric converter was pumped by a Continuum Surlite II non-seeded Nd:YAG laser operating at 10 Hz repetition rate. The typical pulse width of this pump laser is 4−6 ns, with output pulse energy of 600 mJ at 1064 nm. The OPO/OPA laser is tunable within 2800−4000 cm^{-1}, and tunability is achieved by angle fine-adjusting of OPO and OPA crystals simultaneously. The angle tuning is controlled precisely using software-controlled stepping motors. The typical output energy from the OPO/OPA laser was 20 mJ/pulse in the investigated spectral range with 3−4 cm^{-1} bandwidth. IR beam focusing is performed to achieve better overlap with the trapped ion cloud. In the trap, ions were accumulated for 5−50 ms prior to IR irradiation. Multistage mass spectrometry was performed using the standard Bruker Esquire Control (v5.2) software. The typical irradiation time used in the experiment was 0.5−2 s. The irradiation time was controlled using an electromechanical shutter synchronized precisely with the mass spectrometer.

The IRMPD spectrum was obtained by plotting the photofragmentation yield R ($R = -\ln[I_{parent}/(I_{parent} + \sum I_{fragment})]$, where I_{parent} and $I_{fragment}$ are the integrated intensities of the mass peaks of the precursor and of the fragment ions, respectively) as a function of the frequency of the IR radiation.[41] A recent study[42] has demonstrated that this data treatment allows a better comparison with calculated IR absorption spectra and a better spectral resolution than other analysis

methods such as recording a depletion spectrum or calculating a photodissociation yield.

2.3. Computational Details. Molecular orbital calculations were carried out using the B3LYP[43,44] density functional, as implemented in the Gaussian03 set of programs.[45] The different forms considered were optimized with the 6-311G** basis set, without any symmetry constraint. In order to describe the metallic center, we used the Los Alamos effective core potential (ECP) in combination with the LACV3P** basis set.[46−48] Harmonic vibrational frequencies were estimated at this level to characterize the stationary points as local minima or saddle points, and to estimate the zero-point vibrational energy (ZPE) corrections. In the perspective of studying bigger systems, B3LYP/6-31G** calculations were also performed, Pt being described with either the SKBJ ECP+basis sets[49] or the LANL2DZ approach.[46−48] It turned out that both the relative energies and vibrational spectra are similar, regardless of the pseudopotential and basis sets used to perform the calculations.

The IR absorption spectra of the various structures were calculated within the harmonic approximation. As far as the positions of the absorption bands are concerned, a scaling factor value of 0.974 was chosen in the 950−1900 cm^{-1} region, while a value of 0.957 was used in the 2900−3700 cm^{-1} frequency range. Finally, to be consistent with the experimental spectral resolution, the calculated absorption lines were convoluted with a Gaussian profile of 15 cm^{-1} full width at half-maximum (fwhm) in the 950−1900 cm^{-1} region, while a fwhm of 5 cm^{-1} was used for the 2900−3700 cm^{-1} frequency range. As a final point, the relative stability in solution of the various complexes was also evaluated by using the Polarized Continuum Model (PCM) in order to take into account the water solvent.

Throughout this paper, total energies are expressed in hartrees and relative energies in kJ mol^{-1}. For the sake of simplicity, the basis set used for Pt will be referred to as 6-311G**. Detailed geometries (Cartesian coordinates) of all the structures mentioned in this paper are available from the authors upon request.

3. RESULTS AND DISCUSSION

3.1. Collision-Induced Dissociation Experiments. Formation of both *cis*-$[Pt(NH_3)_2(A)Cl]^+$ and *cis*-$[Pt(NH_3)_2(G)Cl]^+$ adducts results from the reaction taking place in a solution containing cisplatin together with either 2′-deoxyadenosine-5′-monophosphate (5′-dAMP) or 2′-deoxyguanosine-5′-monophosphate (5′-dGMP) during a 24 h incubation period. In this process, likely steps comprise the hydration of cisplatin through the displacement of a chloride ion by a water molecule and hydrolysis of the deoxynucleotide. It may be noted that this indirect way of obtaining A and G adducts using a solution containing the corresponding deoxynucleotide as a source of the nucleobase overcomes the problem of the scant solubility of the native nucleobase. The complexes of interest are formed together with other species containing 5′-dGMP or 5′-dAMP or their derivatives bound with cisplatin ions. When the 1:1 mixture of cisplatin and 5′-dGMP is analyzed after 24 h incubation time, under usual ESI conditions, an intense cluster signal is observed at m/z 414−420, consistent with the formation of *cis*-$[Pt(NH_3)_2(G)Cl]^+$ (Figure S1a of the Supporting Information).[50] The simultaneous presence of one chlorine and one platinum atom in the ion yields a characteristic isotopic pattern, easily distinguishable from one corresponding to Pt complexes devoid of a chlorine atom. Under similar conditions, the corresponding *cis*-$[Pt(NH_3)_2(A)Cl]^+$ complex (m/z 398−404) is formed, as evidenced in Figure S1b.

The *cis*-$[Pt(NH_3)_2(G)Cl]^+$ adduct ions have been examined by CID at variable collision energy in a hybrid triple-quadrupole linear ion trap mass spectrometer. The CID spectra were recorded for the selected precursor ion at m/z 415, holding ^{195}Pt and ^{35}Cl isotopes. The variation of the relative abundances of both precursor and fragment ions with respect to the center-of-mass collision energy (E_{CM}) is given in Figure S2 of the Supporting Information. As can be seen from Figure S2, the CID spectrum of the *cis*-$[^{195}Pt(NH_3)_2(G)^{35}Cl]^+$ ion (m/z 415) exhibits a primary fragment at m/z 398 associated with the loss of one molecule of ammonia. One may note that this fragment ion is already present at the lowest collision energy. Four ions are also detected at higher E_{CM}, namely m/z 381, 353, 317, and 152. These fragmentations can be ascribed to subsequent processes originating from the ion at m/z 398.[50] The fragment ion detected at m/z 381 corresponds to loss of the second ammonia molecule, while the ion at m/z 353 is due to the combined elimination of NH_3 and CO. The fragment ion at m/z 317 may be attributed to the elimination of HCl from m/z 353, while the ion detected at m/z 152 corresponds to protonated guanine GH^+.

Likewise the CID of the adenine complex, *cis*-$[Pt(NH_3)_2(A)Cl]^+$, showed similar characteristics. Again, the monoisotopic ion at m/z 399, containing ^{195}Pt and ^{35}Cl, has been mass-selected as precursor ion for CID studies. The variation of the ion intensity of both precursor and fragment ions as a function of E_{CM} is provided in Figure S3 of the Supporting Information. The MS/MS spectrum of the *cis*-$[Pt(NH_3)_2(A)Cl]^+$ complex is characterized by two main dissociation processes. As observed from the guanine complex, the first dissociation product corresponds to the loss of ammonia, yielding the ion at m/z 382. The second one, at m/z 346, is due to the elimination of a HCl molecule. Three additional fragment ions are also detected, which arise from higher energy processes following the primary loss of NH_3. Elimination of a second molecule of ammonia leads to the m/z 365 ion. The species detected at m/z 329 may be attributed to loss of both ammonia and hydrochloric acid, whereas the ion at m/z 136 corresponds to protonated adenine.

From these comparative CID experiments, in the case of *cis*-$[Pt(NH_3)_2(G)Cl]^+$ ion one may envision the presence of a hydrogen bond between a molecule of ammonia of the cisplatin moiety and the guanine carbonyl oxygen, which might account for the fragment ion generated at m/z 353 by the simultaneous loss of ammonia and CO that is peculiar to this complex. Similarly, the concomitant loss of NH_3 and HCl from the *cis*-$[Pt(NH_3)_2(A)Cl]^+$ adduct may suggest the presence of a hydrogen bond between a N−H group of adenine and the Pt-bound chlorine.[50]

To gain a qualitative idea of the energy involved in cisplatin bonding to either adenine or guanine, energy-dependent CID experiments have been performed on ions generated by the loss of the first ammonia molecule. In fact, both ions are found to yield the respective protonated nucleobase by CID. The energy-dependent CID of $[Pt(NH_3)(G)Cl]^+$ is displayed in Figure 1a.

It is worth mentioning that all secondary fragments observed in the MS/MS spectra of *cis*-$[Pt(NH_3)_2(G)Cl]^+$ are present in these CID experiments. Linear extrapolation of the rise of the sigmoid curve yields a phenomenological threshold energy (E_{PT}) of 1.55 ± 0.2 eV (148 ± 20 kJ mol^{-1}) for the appearance of GH^+. Although the breaking of the cisplatin−guanine bond requires a higher energy compared to the other fragments, protonated guanine becomes the principal fragment with increasing E_{CM}. The energy-dependent CID of $[Pt(NH_3)(A)Cl]^+$ is shown in Figure 1b. The value of the phenomenological threshold energy for the appearance of the protonated adenine

dx.doi.org/10.1021/ja309857d | J. Am. Chem. Soc. 2013, 135, 1445−1455

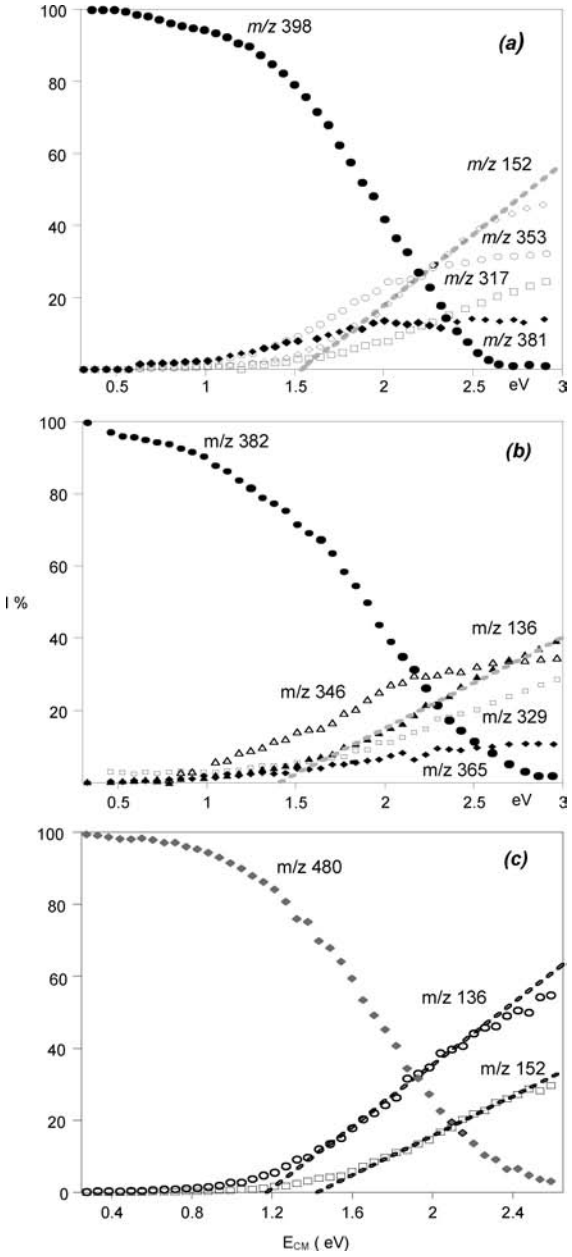

Figure 1. Relative abundances of the precursor ion and fragment ions as a function of the center of mass collision energy (E_{CM}) during CID of mass-selected (a) $[^{195}Pt(NH_3)(G)^{35}Cl]^+$ (m/z 398), (b) $[^{195}Pt(NH_3)(A)^{35}Cl]^+$ (m/z 382), and (c) $[^{195}Pt(A)(G)(-H)]^+$ (m/z 480) ions. See text for details.

ions is 1.38 ± 0.2 eV (132 ± 20 kJ mol^{-1}). Although this extrapolation does not provide, by any means, a direct measure of the threshold energy for dissociation, it suggests that cisplatin is more strongly bound to guanine than to adenine.

As a last piece of information, the mixed complex $[Pt(A)(G)(-H)]^+$ was also studied by CID. Its formation is not trivial. An aqueous solution containing cisplatin, 5′-dGMP, and 5′-dAMP in a 1:1:1 molar ratio needs to be stored at room temperature for more than 20 days in order for the reaction to proceed, yielding the mixed adduct observed by ESI-MS. The full-scan ESI spectrum of this mixture is given in Figure S1c. The solution thus prepared showed two main cluster ions, the first centered around m/z 497, corresponding to adduct $[Pt(NH_3)(A)(G)(-H)]^+$, and the other detected around m/z 480, which corresponds to $[Pt(A)(G)(-H)]^+$. We focused our attention on the latter complex, which may yield insight about whether platinum is preferentially bound to either adenine or guanine. The presence of ammonia in the former complex may induce complicating effects arising from the possibility of hydrogen-bonding interactions between NH_3 and the nucleobases. CID experiments at variable CE have been conducted on the ion at m/z 480, which contains the ^{195}Pt isotope. Two different dissociation channels were observed, leading to protonated adenine and protonated guanine, as displayed in Figure 1c. Phenomenological threshold energy (E_{PT}) values of 1.17 ± 0.20 eV (112 ± 20 kJ mol^{-1}) and 1.46 ± 0.20 eV (140 ± 20 kJ mol^{-1}) are deduced for the fragmentation processes leading to protonated adenine and protonated guanine, respectively. In the event that the energetics of the competitive fragmentation processes were governed by the relative proton affinity of the two bases, a bias could be expected for the formation of protonated guanine. In fact, the gas-phase proton affinity (PA) of guanine (959.5 kJ mol^{-1})[51] is higher than the PA of adenine (942.9 kJ mol^{-1}).[51] Consequently, the CID data would rather suggest that, in the $[Pt(A)(G)(-H)]^+$ complex guanine is more strongly bound than adenine. Thus, one may argue that the preference of cisplatin toward guanine may be related not only to the strong hydrogen bond that can be established between a hydrogen atom of the ammonia ligand and the oxygen atom of guanine (a stronger hydrogen bond than the one involving either N atom of adenine as electron density donor), but also to intrinsic features of the Pt bonding, favoring guanine relative to adenine.

3.2. IRMPD Spectroscopy of *cis*-$[Pt(NH_3)_2(G)Cl]^+$ Complex. The main purpose of this work is to elucidate and characterize the structure of the *cis*-$[Pt(NH_3)_2(G)Cl]^+$ and *cis*-$[Pt(NH_3)_2(A)Cl]^+$ ions, taken as simple models of monoadducts between cisplatin and DNA, by IRMPD spectroscopy. To this end, IRMPD spectra were recorded in two different spectral regions, in the so-called fingerprint region (950−1900 cm^{-1}), using the beamline of the IR-FEL at CLIO, and in the X−H (X = C, N, O) stretching region (2900−3700 cm^{-1}), using a tabletop IR OPO/OPA laser coupled to a modified Paul ion-trap.

In order to extract structural information, the IRMPD spectrum of *cis*-$[Pt(NH_3)_2(G)Cl]^+$ ions is compared with the calculated IR spectra of potential candidate geometries. The optimized structures for isomers corresponding to the *cis*-$[Pt(NH_3)_2(G)Cl]^+$ general formula have been obtained by performing B3LYP/6-311G** calculations and are presented in Figure 2 (all the structures obtained in the present work are gathered in Figures S8 and S9 of the Supporting Information).

Guanine has three possible binding sites with the transition metal, the two nitrogen atoms N3 and N7 and the carbonyl oxygen atom (O6).[52] Insights into the structural features of cisplatin interaction with guanine have been obtained in recent theoretical work. The N7 position of guanine was identified as the preferred platination target.[53] The optimized geometries of *cis*-$[Pt(NH_3)_2(G)Cl]^+$ presented in Figure 2 illustrate the three different binding sites of guanine. Binding to N7 gives rise to two conformers, as also illustrated recently,[53] named **PtGN7-1**, where one hydrogen atom of an ammonia ligand interacts through a hydrogen bond with the carbonyl oxygen at the C6 position, and **PtGN7-2**, where the plane defined by the metal in its square planar coordination is perpendicular to the guanine plane. In fact, the latter structure was actually a transition state at the B3LYP/6-31G** level (one negative eigenvalue).[53] A

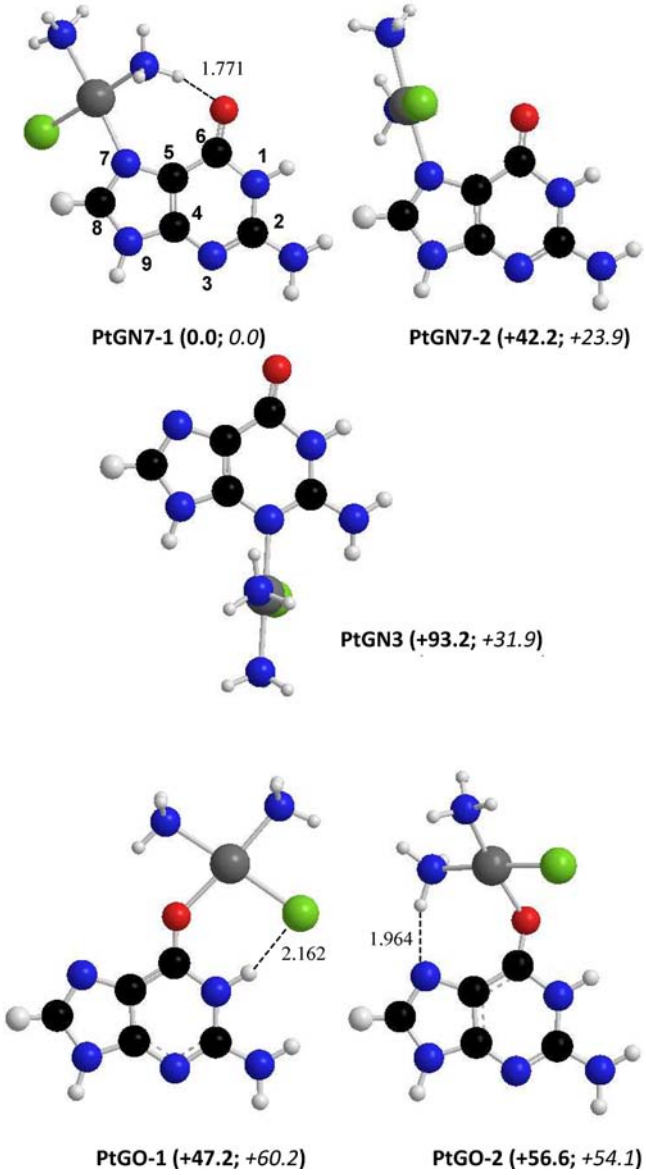

Figure 2. Geometries and relative free energies (kJ mol^{-1}, in parentheses) for representative *cis*-$[Pt(NH_3)_2(G)Cl]^+$ structures calculated at the B3LYP/6-311G** level. Distances are given in angströms. Relative free energies, shown in italics, were obtained by using the Polarized Continuum Model approach.

similar result is obtained with the present level of calculation. Without any constraint, **PtGN7-2** spontaneously evolves toward **PtGN7-1**. The coordination to (O6) yields also two different conformers, differing by the orientation of the $(NH_3)_2Pt(Cl)$ group with respect to the guanine ligand. In the first one, **PtGO-1**, a weak hydrogen bond is found between the hydrogen in N1 and the chloride ligand. In the second one, **PtGO-2**, a hydrogen bond is established between one hydrogen of an ammonia ligand and N7. In another isomer given in Figure 2, **PtGN3**, $(NH_3)_2Pt(Cl)$ is bound to N3. As shown by the relative free energies at 298 K reported in Figure 2, the global minimum corresponds to the **PtGN7-1** complex. The preferred binding site of guanine is N7, yielding a structure that is stabilized by a strong hydrogen bond. When this hydrogen bond is not allowed, the ensuing conformer **PtGN7-2** is only slightly more stable that the O-coordinated structures (**PtGO-1** and **PtGO-2**). Globally, the two latter structures are less stable than **PtGN7-1** by more than 40 kJ mol^{-1}.

Finally, the platination onto the N3 position yields the least stable isomer, placed about 93 kJ mol^{-1} above **PtGN7-1**. Examination of **PtGN3** indicates that the guanine moiety is no longer planar. Consequently, coordination to the N3 atom induces an important distortion of the aromatic ring from planarity that destroys much of the resonance delocalization and is associated with a high-energy species.

In the FT-ICR mass spectrometer, it was possible to isolate the whole isotopic cluster corresponding to the *cis*-$[Pt(NH_3)_2(G)Cl]^+$ complex at m/z 414−418, submitting it to the IRMPD experiment. Fragmentation of *cis*-$[Pt(NH_3)_2(G)Cl]^+$ upon irradiation by IR photons in resonance with an active vibrational mode in the fingerprint region yields the same fragment ions as previously observed in the CID experiments, that is, loss of one NH_3 (cluster at m/z 397−401), loss of two ammonia molecules (cluster at m/z 380−384), and loss of two NH_3 and CO (cluster at m/z 352−356). On the other hand, protonated guanine (m/z 152) is not detected as photofragmentation product (Figure S4 of the Supporting Information). In the X−H stretching region (2900−3700 cm^{-1}), the only photofragment observed in the IRMPD process is $[Pt(NH_3)(G)Cl]^+$ (cluster at m/z 397−401).

The IRMPD spectrum of *cis*-$[Pt(NH_3)_2(G)Cl]^+$ in the 950−1900 cm^{-1} range is plotted in Figure 3a together with the IR spectra calculated for the stable species presented in Figure 2.

The experimental spectrum of *cis*-$[Pt(NH_3)_2(G)Cl]^+$ (Figure 3a) shows four pronounced features at 1289, 1597 1637, and 1718 cm^{-1}, and other weaker bands appear at 1119, 1178, 1213, 1330, 1350, 1428, 1488, and 1536 cm^{-1}.

The main features in the experimental spectrum are nicely matched by the computed spectrum of the isomer **PtGN7-1**. Relying on the typically good agreement between the IRMPD spectrum and the linear IR spectrum of the sampled species obtained by DFT calculations, the vibrational modes of *cis*-$[Pt(NH_3)_2(G)Cl]^+$ can be assigned as described in Table S2, where the experimental IRMPD features are listed together with the IR bands calculated for the most stable isomer **PtGN7-1**. The IR bands calculated for other isomers together with the associated vibrational modes are listed in Tables S3−S5 in the Supporting Information.

The IRMPD feature at 1289 cm^{-1} is particularly broad and presents two shoulders at ca. 1330 and 1350 cm^{-1}. This signal comprises the umbrella bending modes of the two NH_3 ligands. Interestingly, the umbrella mode for the ammonia ligand involved in H-bonding with the carbonyl oxygen in **PtGN7-1** (denoted NH_3 while the other ammonia is called $N'H_3$) is calculated at 1318 cm^{-1}, which may account for the shoulder observed experimentally at 1330 cm^{-1}. The umbrella motion of the $N'H_3$ ligand, trans to G, presents a value at 1301 cm^{-1}. Finally, the shoulder at 1350 cm^{-1}, on the high-frequency side of the IRMPD band at 1289 cm^{-1}, can be assigned to the in-plane bending of H−N1.

The three strong bands at 1597, 1637, and 1718 cm^{-1} are associated to the NH_2 scissoring, the H_2N−C2 stretching, and the C6═O stretching modes calculated at 1597, 1637, and 1706 cm^{-1}, respectively. It is important to note that the C═O stretching is red-shifted with respect to an unperturbed C═O stretching vibration expected at ca. 1810 cm^{-1} as observed in isomer **PtGN3**. This effect can be explained by the formation of a hydrogen bond that weakens the double bond character, and also by the proximity of the platinum ion. Note that the direct

dx.doi.org/10.1021/ja309857d | J. Am. Chem. Soc. 2013, 135, 1445−1455

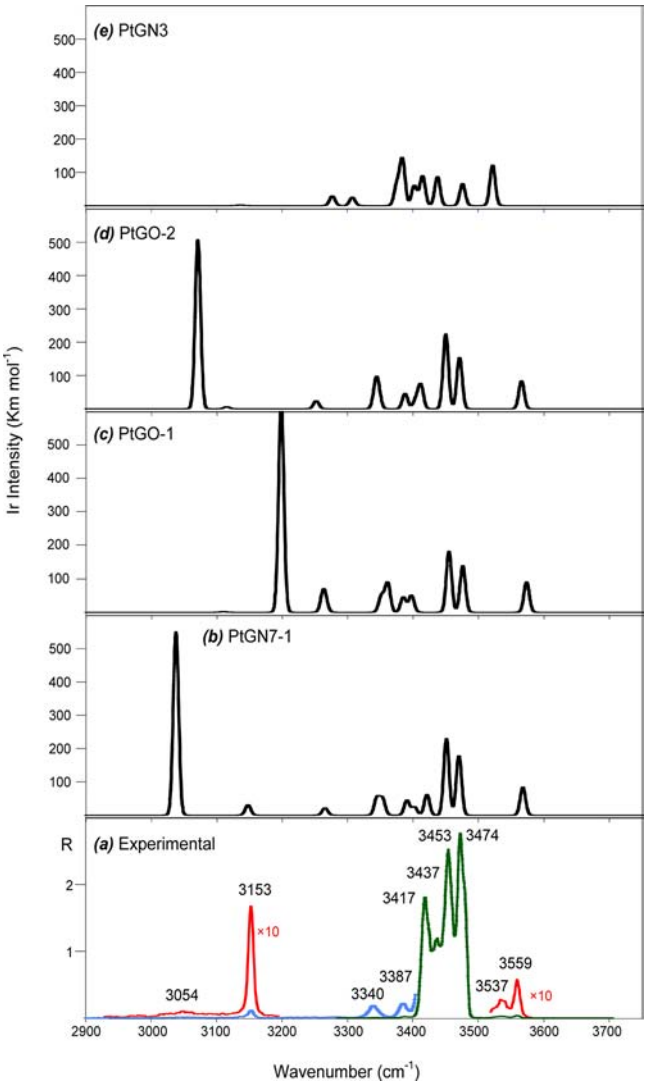

Figure 3. (a) Experimental IRMPD spectrum of *cis*-$[Pt(NH_3)_2(G)Cl]^+$ obtained with full (green) and attenuated (by a factor of 2, red) laser power together with computed IR spectra of (b) **PtGN7-1**, (c) **PTGO-1**, (d) **PtGO-2**, and (e) **PtGN3**, all calculated at the B3LYP/6-311G** level in the spectral range of 950−1900 cm^{-1}.

binding of the platinum ion to the (O6) center further reduces the double bond character of C6═O, and in fact its absorption is red-shifted to 1656 cm^{-1} (**PtGO-1** structure, Table S4). Conversely, the H_2N−C2 stretching mode is blue-shifted due to the partial double-bond character of the N−C2 bond, as attested by the sp^2 hybridization of the NH_2 group. The other minor absorptions can be assigned to vibrational modes of the purine ring and are reported in detail in Table S2. As a further remark on the IRMPD spectrum of *cis*-$[Pt(NH_3)_2(G)Cl]^+$ in the fingerprint region, one may note that recording the spectrum with an attenuated beam (thus reducing saturation effects) brings the relative band intensities in better agreement with the calculated IR spectrum of **PtGN7-1**.

Examination of Figure 3 shows that the IR signatures of **PtGO-1** or **PtGO-2** forms are also globally consistent with the experimental spectrum and, consequently, cannot be rigorously excluded. However, these two structures are significantly less stable than **PtGN7** in the gas phase. In addition, PCM calculations were also carried out onto these complexes in order to get some insight about the effect of the solvent. These calculations show that the energy gap between these three forms should be further increased in water, which is consistent with the prominent formation of **PtGN7** during the ESI process, if one considers that the ion population will reflect the Boltzmann equilibrium distribution in water.

The *cis*-$[Pt(NH_3)_2(G)Cl]^+$ ions have also been investigated in the region from 2900 to 3700 cm^{-1}. As shown in the lower panel of Figure 4, *cis*-$[Pt(NH_3)_2(G)Cl]^+$ presents numerous absorptions, the four major ones being observed at 3417, 3437, 3453, and 3474 cm^{-1}.

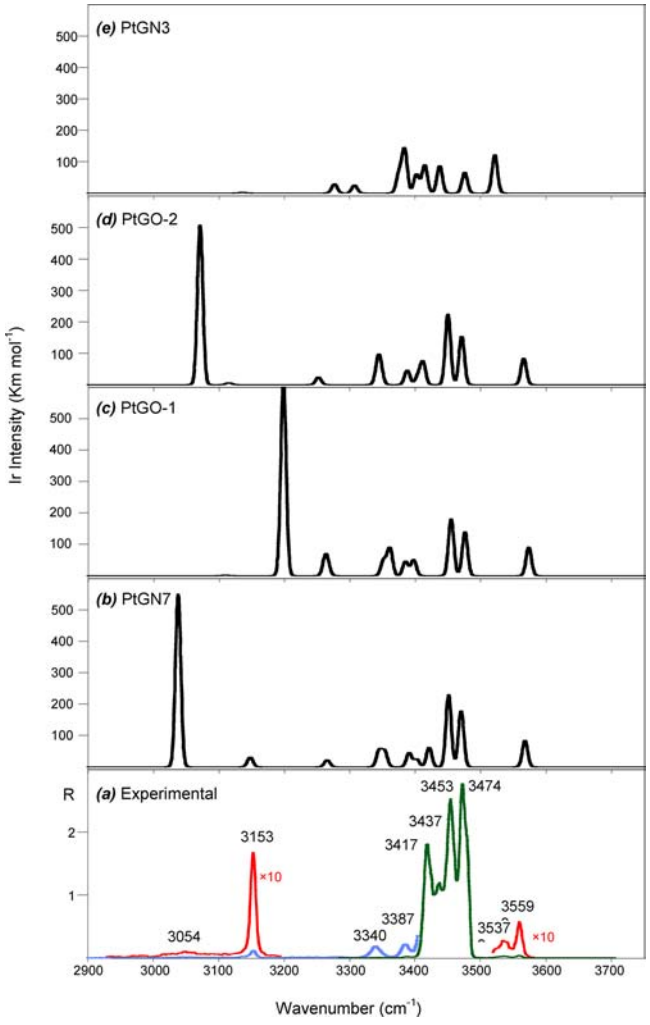

Figure 4. (a) Experimental IRMPD spectrum of *cis*-$[Pt(NH_3)_2(G)Cl]^+$ obtained with irradiation times of 1 s (green) and 2 s (blue), together with computed IR spectra of (b) **PtGN7-1**, (c) **PTGO-1**, (d) **PtGO-2**, and (e) **PtGN3**, all calculated at the B3LYP/6-311G** level in the spectral range of 2900−3700 cm^{-1}.

Other weaker but still significant features are detected at 3054, 3153, 3340, 3387, 3537, and 3559 cm^{-1}. Once again, on comparing with the calculated IR spectra convoluted with a Gaussian profile of 5 cm^{-1} (fwhm) reported in Figure 4b−e, one finds a generally good agreement between the IRMPD spectrum of *cis*-$[Pt(NH_3)_2(G)Cl]^+$ and the IR spectrum of isomer **PtGN7-1**. The main feature at 3474 cm^{-1} can be assigned to the N9−H stretching mode expected at 3470 cm^{-1}. The absorption at 3417 cm^{-1} corresponds to the N1−H stretching mode calculated at 3421 cm^{-1}. The two bands at 3453 and 3559 cm^{-1} are consistent with the symmetric and

dx.doi.org/10.1021/ja309857d | J. Am. Chem. Soc. 2013, 135, 1445−1455

antisymmetric stretching modes of NH_2 expected at 3451 and 3567 cm^{-1}, respectively, for **PtGN7-1**. The two bands at 3340 and 3387 cm^{-1} are due to antisymmetric stretching modes of the NH_3 ligands. The first one comprises two absorptions calculated at 3345 and 3353 cm^{-1}, and the second one is a convolution of modes active at 3393 and 3401 cm^{-1}. The feature at 3153 cm^{-1} is compatible with the C8−H stretching mode expected at 3148 cm^{-1}. The experimental IRMPD spectrum of *cis*-$[Pt(NH_3)_2(G)Cl]^+$ shows a broad absorption around 3054 cm^{-1} that may be assigned to the NH stretching of the N−H bond involved in hydrogen-bonding with the carbonyl oxygen of guanine, calculated at 3038 cm^{-1}. Although the calculated intensity for this stretching mode involving hydrogen bonding is high, the experimental band is rather weak. Previously, such simultaneous red-shifts and broadening effects of stretching vibrations of X−H (X = N,O) groups involved in a hydrogen bond have been observed for water-solvated clusters,[54] solvated amino acids[55] or nucleobases,[56,57] and lactic ester derivatives.[58] One possible explanation may lie in the anharmonicity of this mode and the ensuing low IRMPD efficiency. However, the presence of these two latter features is remarkable. To our knowledge, this is one of the first examples of NH vibration involved in hydrogen bonding revealed by IRMPD spectroscopy using an OPO/OPA laser, in the absence of a loosely bound tag such as a solvating water molecule.[54] It is also difficult to observe C−H stretching modes for covalently bonded species with the present experimental apparatus. Typically, these modes are weakly active, and at the same time the laser power at wavenumbers lower than 3100 cm^{-1} is appreciably decreasing.

It may be noted that the experimental spectrum of *cis*-$[Pt(NH_3)_2(G)Cl]^+$ shows two features that do not find a counterpart in the calculated IR spectrum of isomer **PtGN7-1**, namely the bands at 3437 and 3537 cm^{-1}. These signals can be compared with two absorptions bands computed for the **PtGN7-2** conformer, at 3435 and 3553 cm^{-1}, respectively, corresponding to the symmetric and antisymmetric stretching modes of NH_2 as reported in Figure S5 in the Supporting Information. Considering the high relative free energy of **PtGN7-2** with respect to **PtGN7-1** (higher than 42 kJ mol^{-1}), and given the fact that this structure is actually a transition state on the potential energy surface, it is somewhat difficult to conceive the presence of the **PtGN7-2** in any significant amount from the ESI process. More probably, these two relatively minor absorptions may arise from a conformer that has been missed in the conformational survey. Whatever the right explanation could be, the observed features appear consistent with an isomer characterized by *cis*-$[Pt(NH_3)_2Cl]^+$ binding to guanine in the N7 position.

3.3. IRMPD Spectroscopy of the *cis*-$[Pt(NH_3)_2(A)Cl]^+$ Complex. The last issue addressed in this work regards the structure of the *cis*-$[Pt(NH_3)_2(A)Cl]^+$ complex generated in the water solution. Contrary to guanine, the three possible binding sites of adenine, namely N1, N3 and N7, show quite similar affinity for the platinum moiety. The calculated binding affinity order for $[Pt(NH_3)_3]^{2+}$ was N3 (368.2 kJ mol^{-1}) ≥ N1 (364.0 kJ mol^{-1}) > N7 (338.9 kJ mol^{-1}).[52] In DNA, cisplatin binds the adenine residue especially onto N7 and N1 positions. However, dealing with the nucleobase alone, the three positions are all potentially available for the cisplatin interaction. Furthermore, previous studies have demonstrated that adenine can tautomerize in water and polar solvents.[59,60] NMR measurements in water have established the coexistence of two amino tautomers of adenine, namely the N9−H tautomer (so-called native adenine, predominant by a factor of ca. 4) and the N7−H structure.[61] The presence of the N3−H form, though in only minor amount, has been detected exclusively in DMSO solvent.[59] For this reason, in addition to the conventional binding sites of canonical adenine, complexes of $(NH_3)_2Pt(Cl)^+$ with the N7−H tautomers have also been considered as potential candidates for the *cis*-$[Pt(NH_3)_2(A)Cl]^+$ complex obtained in aqueous solution. Figure 5 displays the optimized structures of the most stable conformer for plausible *cis*-$[Pt(NH_3)_2(A)Cl]^+$ isomers as obtained at the B3LYP/6-311G** level.

The **PtAN3** structure illustrates the most stable conformer obtained by the interaction of the $(NH_3)_2PtCl^+$ unit with the N3 position of native adenine. The chloride ion is pointing

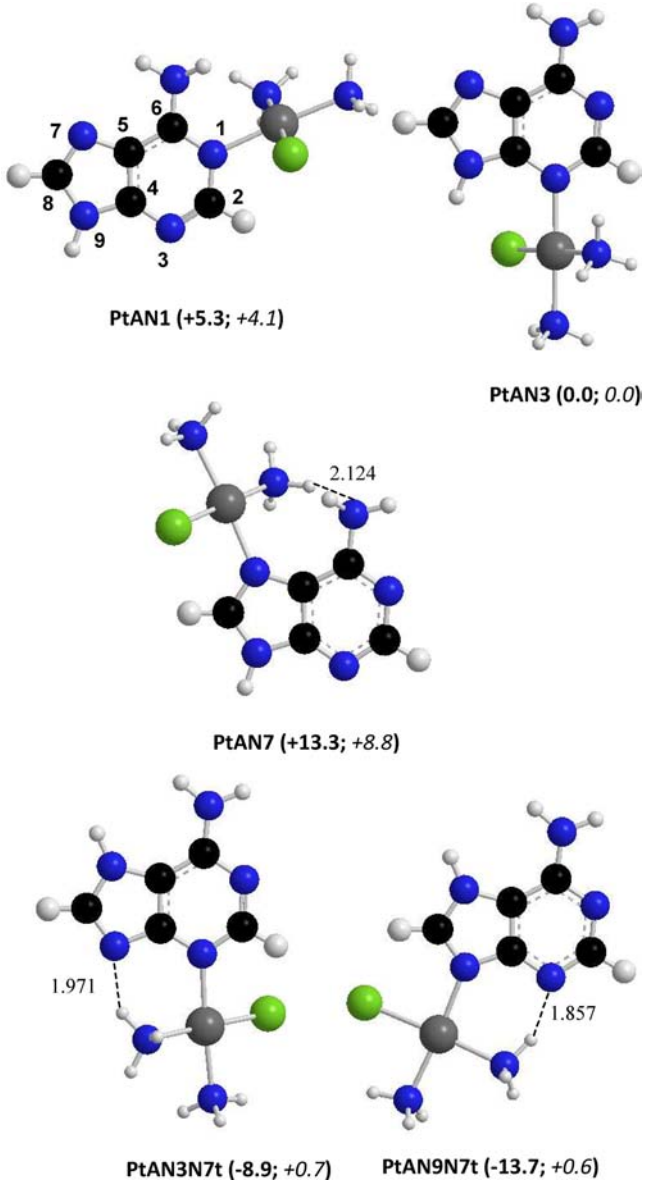

Figure 5. Geometries and relative free energies (kJ mol^{-1}, in parentheses) for representative *cis*-$[Pt(NH_3)_2(A)Cl]^+$ structures calculated at the B3LYP/6-311G** level. Distances are given in angströms. Relative free energies, shown in italics, were obtained by using the Polarized Continuum Model approach.

dx.doi.org/10.1021/ja309857d | J. Am. Chem. Soc. 2013, 135, 1445−1455

toward the hydrogen atom in N9. The distance between the two atoms (2.723 Å) is too large to allow proper H-bonding; however, it may provide stabilization by an electrostatic effect. The binding to N1 and N7 positions of adenine in the native form yields structures **PtAN1** and **PtAN7**, respectively (Figure 5). In the N7−H amino tautomer of adenine, binding to N3 yields **PtAN3N7t** also shown in Figure 5. In this structure, a hydrogen bond is established between a hydrogen of an ammonia ligand and N9. The **PtAN9N7t** form, obtained by the coordination of $Pt(NH_3)_2Cl^+$ to N9 of the N7−H tautomer, also allows hydrogen-bonding between a hydrogen of an ammonia ligand and N3.

Focusing on the three isomers of the *cis*-$[Pt(NH_3)_2(A)Cl]^+$ complexes involving native adenine, binding to N3 gives rise to the lowest energy isomer. In agreement with previous calculations,[52] **PtAN1** is only 5.3 kJ mol^{-1} less stable than **PtAN3**, and the coordination to N7 (**PtAN7**) is less favored by 13.3 kJ mol^{-1}. Unexpectedly, the two structures of *cis*-$[Pt(NH_3)_2(A)Cl]^+$ involving tautomer N7−H are lower in energy with respect to **PtAN3**. This result may appear surprising because native adenine is calculated to be the most stable tautomer.[59,62] A probable explanation lies in the presence of a hydrogen bond in both **PtAN3N7t** and **PtAN9N7t** complexes, providing additional stabilization to these species. The lowest energy isomer is thus **PtAN9N7t**, 13.7 kJ mol^{-1} more stable than **PtAN3**. On the other hand, PCM calculations suggest **PtAN3** as the most stable structure in solution, the energy difference between the various forms being strongly reduced (Figure 5).

As in the case of *cis*-$[Pt(NH_3)_2(G)Cl]^+$, the whole isotopic cluster corresponding to the *cis*-$[Pt(NH_3)_2(A)Cl]^+$ complex at m/z 398−404 was isolated prior to starting the IRMPD experiment. The photofragmentation efficiency observed for *cis*-$[Pt(NH_3)_2(A)Cl]^+$ was lower than in the case of *cis*-$[Pt(NH_3)_2(G)Cl]^+$ in both spectroscopic regions investigated (resulting in smaller R values).

In the fingerprint region there are only four photofragment ions observed, as reported in Figure S6 in the Supporting Information. The principal fragment ion is the one from loss of one NH_3 (cluster at m/z 381−387), and a second abundant one is the protonated adenine at m/z 136. A less abundant photofragment is due to loss of one ammonia plus a hydrogen chloride molecule (cluster at m/z 345−347). This ion tends to add a molecule of water, present as unavoidable contaminant in the Paul trap (cluster at m/z 365−367). The same ionic products are observed for photodissociation in the X−H stretching region (2900−3700 cm^{-1}). It should be noted that, in contrast with the behavior displayed by *cis*-$[Pt(NH_3)_2(G)Cl]^+$, protonated adenine is always present as a photofragment. This fact is in line with a stronger binding of guanine with respect to adenine in platinum complexes.

The IRMPD spectrum of *cis*-$[Pt(NH_3)_2(A)Cl]^+$ recorded in the 1000−1900 cm^{-1} spectral range is reported in the lower panel of Figure 6, together with the calculated IR spectra of the species shown in Figure 5.

Even using a longer irradiation time (1 s instead of 250 ms), the photofragmentation process is considerably less extensive than that observed for *cis*-$[Pt(NH_3)_2(G)Cl]^+$. Three main features are present in the spectrum of *cis*-$[Pt(NH_3)_2(A)Cl]^+$ at 1300, 1430, and 1658 cm^{-1}, respectively. The latter absorption is preceded by a shoulder at 1610 cm^{-1}. Other weaker bands are found at 1120, 1208, 1256, 1361, and 1494 cm^{-1}. Apparently, all the calculated spectra displayed in Figure 6

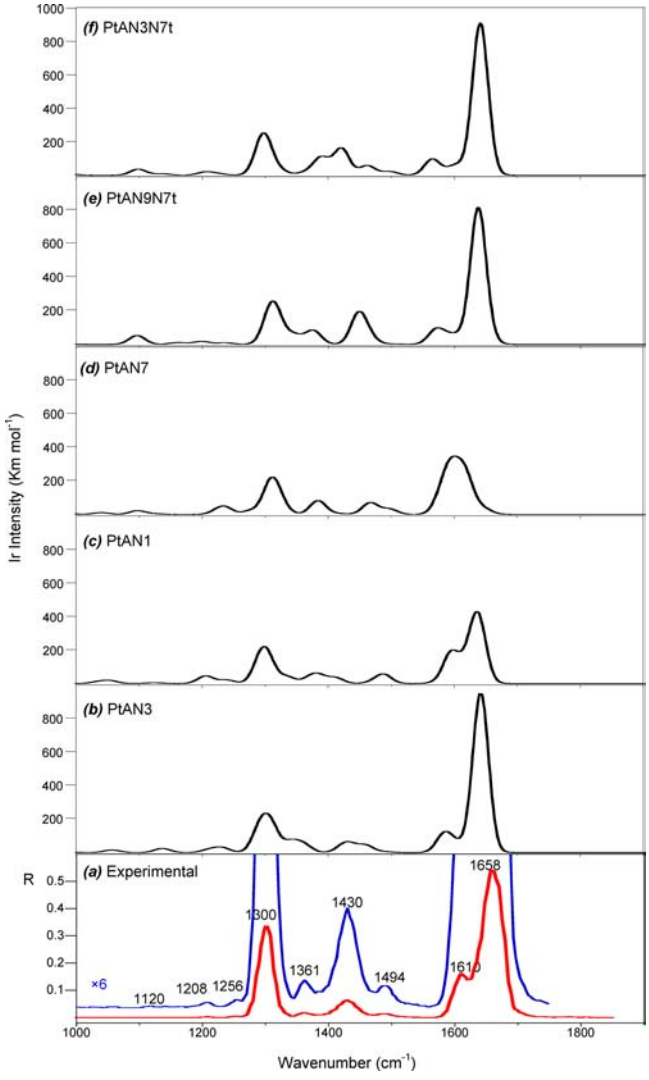

Figure 6. (a) Experimental IRMPD spectrum of *cis*-$[Pt(NH_3)_2(A)Cl]^+$ together with computed IR spectra of (b) **PtAN3**, (c) **PtAN1**, (d) **PtAN7**, (e) **PtAN9N7t**, and (f) **PtAN3N7t**, all calculated at the B3LYP/6-311G** level, in the spectral range of 1000−1900 cm^{-1}.

seem to be very similar to each other and well related to the experimental one. However, some minor differences in the calculated spectra may allow an insight about the sampled ion population. At first sight, one may exclude the presence of **PtAN7** in the *cis*-$[Pt(NH_3)_2(A)Cl]^+$ experimental ion population. The band calculated at about 1602 cm^{-1}, combining two highly active vibrational modes at 1594 and 1616 cm^{-1}, is notably shifted with respect to the experimental one found at 1658 cm^{-1}. In contrast, all other four species taken in consideration present a strong feature at nearly constant frequency, namely at 1641, 1638, 1639, and 1642 cm^{-1} for **PtAN3N7t**, **PtAN9N7t**, **PtAN1**, and **PtAN3**, respectively. As another criterion helping to assign the proper structure, one may consider the gap between this feature and the band preceding it. In the two isomers of tautomer N7−H, the difference in the band position is 76 cm^{-1} for **PtAN3N7t** (at 1565 and 1641 cm^{-1}) and 67 cm^{-1} for **PtAN9N7t** (the two bands are predicted at 1571 and 1638 cm^{-1}). These two values are significantly greater than the gap observed experimentally (48 cm^{-1}), rather disproving the presence of these two species in relevant amounts in the sampled *cis*-$[Pt(NH_3)_2(A)Cl]^+$ ions.

dx.doi.org/10.1021/ja309857d | J. Am. Chem. Soc. 2013, 135, 1445−1455

The calculated spectrum of **PtAN3** gives the best fit with the experimental spectrum. The gap between the two absorptions in the higher frequency region of the mid-IR spectrum is 55 cm^{-1}, in quite good agreement with the experimental value of 48 cm^{-1}. The band at 1361 cm^{-1} finds a counterpart in the calculated mode at ca. 1355 cm^{-1}, associated with the convolution of two bands at 1341 and 1362 cm^{-1}. There is also a good agreement with other features of the spectrum. Only two experimental IRMPD bands do not find a counterpart in the calculated spectrum of isomer **PtAN3**, the small absorption at 1494 cm^{-1}, as well as the band at 1208 cm^{-1}, which, however, can both be observed in the calculated spectrum of isomer **PtAN1**, at 1488 and 1206 cm^{-1}, respectively. **PtAN1** shows a separation of 45 cm^{-1} in the position of the two bands at around 1600 cm^{-1}, in accord with the experimental spectrum. These findings suggest that the ionic adduct *cis*-$[Pt(NH_3)_2(A)Cl]^+$ under examination would be a mixture of both isomers **PtAN3** and **PtAN1**. In addition, several argument are in favor of a minor, if any, contribution of complexes containing N7−H tautomers. First, as previously reported,[59,60] native adenine is the major species in water solution, and PCM calculations suggest that the most stable *cis*-$[Pt(NH_3)_2(A)Cl]^+$ complex (**PtAN3**) involves native adenine. Second, due to the poor solubility of adenine, an aqueous solution of 5′-dAMP rather than of adenine was used in the present study to generate *cis*-$[Pt(NH_3)_2(A)Cl]^+$. Reported NMR measurements of AMP in water solution have found that this species, in contrast with adenine, does not tautomerize.[59] One may therefore argue that, in solution, *cis*-$[Pt(NH_3)_2(H_2O)Cl]^+$ is reacting with 5′-dAMP, and in the event of ion transfer to the gas phase during the electrospray process, direct N-glycosidic bond cleavage occurs, yielding native adenine-containing *cis*-$[Pt(NH_3)_2(A)Cl]^+$ ion.

With these considerations in mind, the vibrational modes of *cis*-$[Pt(NH_3)_2(A)Cl]^+$ can be in a first attempt assigned as described in Table S6, where the experimental IRMPD features are listed together with the IR bands calculated for **PtAN3**. Focusing on the main absorptions, the experimental band at 1300 cm^{-1} can be assigned to the umbrella mode of the ammonia ligands calculated at 1295 and 1310 cm^{-1}. The principal feature at 1658 cm^{-1} can be related to the combination of two vibrational modes, namely the NH_2 scissoring and the C6−NH_2 stretching, expected at 1642 cm^{-1}. Finally, the shoulder at 1610 cm^{-1} may correspond to NH_2 scissoring combined with ring deformation modes, computed at 1582 and 1588 cm^{-1}, respectively.

To complete this study, the IRMPD spectrum of *cis*-$[Pt(NH_3)_2(A)Cl]^+$ has also been recorded in the 3000−3700 cm^{-1} spectral range, using an irradiation time of 2 s and the full laser power in order to maximize the photofragmentation yield. As reported in the lower panel of Figure 7, the experimental IRMPD spectrum of *cis*-$[Pt(NH_3)_2(A)Cl]^+$ presents three main absorptions at 3353, 3428, and 3477 cm^{-1} and two shoulders at 3375 and 3456 cm^{-1}.

The spectrum is consistent with the presence of both **PtAN3** and **PtAN1** isomers in the sampled *cis*-$[Pt(NH_3)_2(A)Cl]^+$ ion population, although some calculated IR bands of expected lower activity are missing in the experimental spectrum. The main feature at 3428 cm^{-1} is in good agreement with the symmetric stretching of NH_2 expected at 3430 cm^{-1} for **PtAN3** isomer (Table S6). The large band at 3477 cm^{-1} can be assigned to a convolution of two vibrational modes of **PtAN1** isomer, namely the N9−H stretching mode and the asymmetric

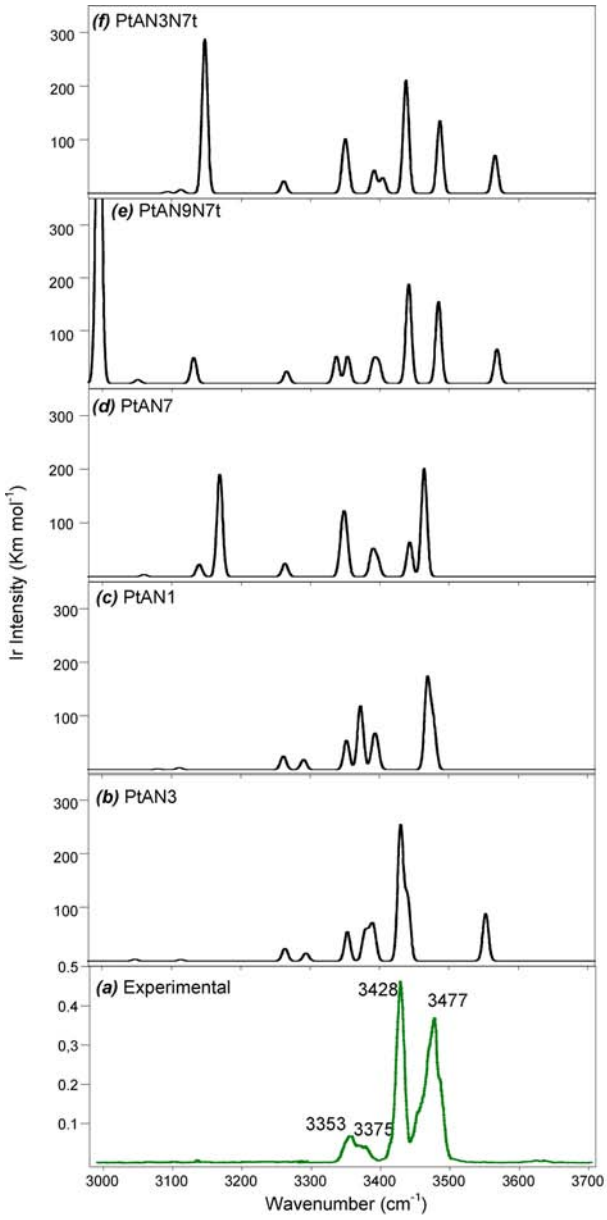

Figure 7. (a) Experimental IRMPD spectrum of *cis*-$[Pt(NH_3)_2(A)Cl]^+$ together with computed IR spectra of (b) **PtAN3**, (c) **PtAN1**, (d) **PtAN7**, (e) **PtAN9N7t**, and (f) **PtAN3N7t**, all calculated at the B3LYP/6-311G** level, in the spectral range of 3000−3700 cm^{-1}.

stretching mode of NH_2 calculated at 3469 and 3478 cm^{-1}, respectively. The small hump at about 3456 cm^{-1} is compatible with the N9−H stretching mode of **PtAN3** estimated at 3440 cm^{-1}. The absorption at 3353 cm^{-1} with a large shoulder at around 3375 cm^{-1} corresponds to stretching modes of NH_3 groups pertaining to both isomers, expected at 3353, 3379, 3386, and 3382 cm^{-1} for **PtAN3** and 3352, 3372, 3374, 3392, and 3396 cm^{-1} for **PtAN1**. Regrettably, the calculated band at 3553 cm^{-1}, which corresponds to the asymmetric stretching mode of NH_2 of **PtAN3** isomer, is not observed in the experimental spectrum. The absence of this band is not easy to explain; however, it may be noted that this mode is very weak also in the experimental spectrum of *cis*-$[Pt(NH_3)_2(G)Cl]^+$, which has a much better IRMPD response. Such a weak asymmetric NH_2 stretch has already been observed for Li^+/

dx.doi.org/10.1021/ja309857d | J. Am. Chem. Soc. 2013, 135, 1445−1455

adenine/thymine complexes[28,29] and protonated dimers of adenine.[63]

A further experiment has finally demonstrated that the two main absorptions at 3428 and 3477 cm^{-1} do not belong to a single structure, as is the case for the calculated spectra of **PtAN3N7t** and **PtAN9N7t**. Two IRMPD spectra of *cis*-$[Pt(NH_3)_2(A)Cl]^+$ were recorded on the same day, the first one using a "fresh" solution where cisplatin and 5′-dAMP had been allowed to react for 24 h before the analysis (Figure S7a), and the second one using an "old" solution where the two substrates had been incubated for 2 weeks (Figure S7b). The result was revealing. The IRMPD spectrum of the "fresh" solution was identical to the one reported in Figure 7. The experimental spectrum of the "old" solution instead showed a noticeable reversal in the relative intensities of the two main peaks as reported in Figure S7. The band at 3428 cm^{-1} is now weaker, and the feature at 3477 cm^{-1} becomes the principal absorption. In our opinion, this fact is evidence that the two main bands pertain to at least two isomers. In fact, with a single isomer present, the same IRMPD spectrum should be recorded with characteristic band positions and intensities. This is indeed the case for the *cis*-$[Pt(NH_3)_2(G)Cl]^+$ complex, showing constantly high reproducibility in IRMPD spectra run on different solutions and different days. In the specific case of *cis*-$[Pt(NH_3)_2(A)Cl]^+$, the inversion of the intensities of the two bands suggests a slow isomerization within the complex. Studying the mechanisms associated with this isomerization is beyond the scope of the present manuscript and will be the subject of further investigation. Clearly, it is noteworthy to underline that all the other experiments reported in the present paper were done only with "fresh" solutions, and thus can be referred to the same ionic population.

Certainly, the presence of N7−H tautomeric forms for the *cis*-$[Pt(NH_3)_2(A)Cl]^+$ complex cannot be rigorously excluded, notably given their particular calculated stability both in solution and in the gas phase. As suggested by one of the reviewers, and as already nicely illustrated for peptides,[64] isotopic labeling with ^{15}N, selectively introduced onto the N7 and N9 positions of 5′-dAMP, would provide useful information in order to definitely attribute the various N−H stretches (red-shifts) and would address the presence of isomeric forms, and especially tautomers. According to our DFT calculations, red-shifts of about 8−9 cm^{-1} should be observed for the N7−H and N9−H stretches. Unfortunately, these compounds are not easily available.

4. CONCLUSIONS

The aim of this study was to provide an accurate characterization of *cis*-$[Pt(NH_3)_2(G)Cl]^+$ and *cis*-$[Pt(NH_3)_2(A)Cl]^+$, models of the monofunctional adducts between cisplatin and the nucleobases of DNA, using IR spectroscopy of ions directly performed in the cell of a mass spectrometer. Both the IR characterization and the computational results point to a covalent structure for *cis*-$[Pt(NH_3)_2(G)Cl]^+$ where Pt is uniformly bound to the N7 atom of guanine. In particular, the feature found at 1718 cm^{-1}, corresponding to the C═O stretching, notably red-shifted with respect to an unperturbed C═O stretching vibration, and the absorption at 3054 cm^{-1}, pertaining to the N−H stretching of the NH_3 molecule involved in hydrogen bonding with the carbonyl oxygen of guanine, are clear proof of the existence of a strong hydrogen bond between the carbonyl group at the C6 position of guanine and the H atom of one NH_3 ligand of cisplatin in the Pt−guanine complex.

The IRMPD spectra of *cis*-$[Pt(NH_3)_2(A)Cl]^+$ are consistent with the presence of two major isomers, **PtAN3** and **PtAN1**, where Pt is bound in the N3 and N1 positions of native adenine, respectively.

The preferred platinum coordination site on adenine seems to be N3, which is not observed in the cell because such a site is located in the internal groove and not easily accessible at an intrastrand cross-linking. However, this feature may open the way toward new transplatin compounds with a conformation potentially allowing an intrastrand cross-link between the N7 position of guanine and the N3 position of adenine.

■ ASSOCIATED CONTENT

Ⓢ Supporting Information

Complete ref 45; detailed experimental mass spectra; CID and IRMPD spectra of ions under examination; tables with experimental and computed vibrational bands; and computed structures for *cis*-$[Pt(NH_3)_2(G)Cl]^+$ and *cis*-$[Pt(NH_3)_2(A)Cl]^+$. This material is available free of charge via the Internet at http://pubs.acs.org.

■ AUTHOR INFORMATION

Corresponding Author

barbara.chiavarino@uniroma1.it; jean-yves.salpin@univ-evry.fr

Notes

The authors declare no competing financial interest.

■ ACKNOWLEDGMENTS

The authors thank the CLIO team (J. M. Ortega, C. Six, G. Perilhous, J. P. Berthet) as well as P. Maître and V. Steinmetz for their support during the experiments. Financial support has been provided by the Italian MIUR (Prin project 2009W2W4YF_004) and by the European Union (project IC007-11 entitled "The interaction of cisplatin with nucleic acids: an approach by IRMPD spectroscopy").

■ REFERENCES

(1) *Platinum and Other Metal Coordination Compounds in Cancer Chemotherapy*; Howell, S. B., Ed.; Plenum Press: New-York, 1996.
(2) Rosenberg, B.; Van Camp, L.; Krigas, T. *Nature* **1965**, *205*, 698.
(3) Rosenberg, B.; Vancamp, L.; Trosko, J. E.; Mansour, V. H. *Nature* **1969**, *222*, 385.
(4) Jamieson, E. R.; Lippard, S. J. *Chem. Rev.* **1999**, *99*, 2467.
(5) Boulikas, T.; Pantos, A.; Bellis, E.; Christofis, P. *Cancer Ther.* **2007**, *5*, 537.
(6) Sherman, S. E.; Lippard, S. J. *Chem. Rev.* **1987**, *87*, 1153.
(7) Bancroft, D. P.; Lepre, C. A.; Lippard, S. J. *J. Am. Chem. Soc.* **1990**, *112*, 6860.
(8) Sherman, S. E.; Gibson, D.; Wang, A. H.; Lippard, S. J. *Science* **1985**, *230*, 412.
(9) Sherman, S. E.; Gibson, D.; Wang, A. H. J.; Lippard, S. J. *J. Am. Chem. Soc.* **1988**, *110*, 7368.
(10) Chiavarino, B.; Crestoni, M. E.; Fornarini, S.; Lemaire, J.; Maitre, P.; MacAleese, L. *J. Am. Chem. Soc.* **2006**, *128*, 12553.
(11) Chiavarino, B.; Crestoni, M. E.; Fornarini, S.; Dopfer, O.; Lemaire, J.; Maitre, P. *J. Phys. Chem. A* **2006**, *110*, 9352.
(12) Brodbelt, J. S.; Wilson, J. J. *Mass Spectrom. Rev.* **2009**, *28*, 390.
(13) Coletti, C.; Re, N.; Scuderi, D.; Maitre, P.; Chiavarino, B.; Fornarini, S.; Lanucara, F.; Sinha, R. K.; Crestoni, M. E. *Phys. Chem. Chem. Phys.* **2010**, *12*, 13455.
(14) Sinha, R. K.; Chiavarino, B.; Crestoni, M. E.; Scuderi, D.; Fornarini, S. *Int. J. Mass Spectrom.* **2011**, *308*, 209.

(15) Chiavarino, B.; Crestoni, M. E.; Dopfer, O.; Maitre, P.; Fornarini, S. *Angew. Chem., Int. Ed.* **2012**, *51*, 4947.
(16) Chiavarino, B.; Crestoni, M. E.; Fornarini, S.; Lanucara, F.; Lemaire, J.; Maitre, P.; Scuderi, D. *Int. J. Mass Spectrom.* **2008**, *270*, 111.
(17) Kapota, C.; Lemaire, J.; Maitre, P.; Ohanessian, G. *J. Am. Chem. Soc.* **2004**, *126*, 1836.
(18) Polfer, N. C.; Oomens, J.; Dunbar, R. C. *Phys. Chem. Chem. Phys.* **2006**, *8*, 2744.
(19) Dunbar, R. C.; Polfer, N. C.; Oomens, J. *J. Am. Chem. Soc.* **2007**, *129*, 14562.
(20) MacAleese, L.; Maitre, P. *Mass Spectrom. Rev.* **2007**, *26*, 583.
(21) Polfer, N. C.; Oomens, J.; Dunbar, R. C. *ChemPhysChem* **2008**, *9*, 579.
(22) Balaj, O. P.; Kapota, C.; Lemaire, J.; Ohanessian, G. *Int. J. Mass Spectrom.* **2008**, *269*, 196.
(23) Bush, M. F.; Oomens, J.; Saykally, R. J.; Williams, E. R. *J. Am. Chem. Soc.* **2008**, *130*, 6463.
(24) Gillis, E. A. L.; Rajabi, K.; Fridgen, T. D. *J. Phys. Chem. A* **2009**, *113*, 824.
(25) Eyler, J. R. *Mass Spectrom. Rev.* **2009**, *28*, 448.
(26) Polfer, N. C.; Oomens, J. *Mass Spectrom. Rev.* **2009**, *28*, 468.
(27) Zocher, E.; Sigrist, R.; Chen, P. *Inorg. Chem.* **2007**, *46*, 11366.
(28) Gillis, E. A. L.; Fridgen, T. D. *Int. J. Mass Spectrom.* **2010**, *297*, 2.
(29) Rajabi, K.; Gillis, E. A. L.; Fridgen, T. D. *J. Phys. Chem. A* **2010**, *114*, 3449.
(30) Salpin, J. Y.; Guillaumont, S.; Ortiz, D.; Tortajada, J.; Maitre, P. *Inorg. Chem.* **2011**, *50*, 7769.
(31) Salpin, J. Y.; Gamiette, L.; Tortajada, J.; Besson, T.; Maitre, P. *Int. J. Mass Spectrom.* **2011**, *304*, 154.
(32) Chiavarino, B.; Crestoni, M. E.; Fornarini, S.; Taioli, S.; Mancini, I.; Tosi, P. *J. Chem. Phys.* **2012**, *137*, 024307.
(33) Schröder, D.; Schwarz, H.; Aliaga-Alcalde, N.; Neese, F. *Eur. J. Inorg. Chem.* **2007**, 816.
(34) Schröder, D.; Semialjac, M.; Schwarz, H. *Int. J. Mass Spectrom.* **2004**, *233*, 103.
(35) Chiavarino, B.; Crestoni, M. E.; Fornarini, S.; Lanucara, F.; Lemaire, J.; Maitre, P.; Scuderi, D. *Chem.—Eur. J.* **2009**, *15*, 8185.
(36) Armentrout, P. B. *Int. J. Mass Spectrom.* **2003**, *227*, 289.
(37) Armentrout, P. B.; Kickel, B. L. In *Organometallic Ion Chemistry*; Freiser, B. S., Ed.; Kluwer Academic Publishers: Dordrecht, 1996.
(38) Milko, P.; Roithova, J.; Schroder, D.; Lemaire, J.; Schwarz, H.; Holthausen, M. C. *Chem.—Eur. J.* **2008**, *14*, 4318.
(39) Bouchoux, G.; Salpin, J. Y.; Leblanc, D. *Int. J. Mass Spectrom. Ion Processes* **1996**, *153*, 37.
(40) Bakker, J. M.; Besson, T.; Lemaire, J.; Scuderi, D.; Maitre, P. *J. Phys. Chem. A* **2007**, *111*, 13415.
(41) Lemaire, J.; Boissel, P.; Heninger, M.; Mauclaire, G.; Bellec, G.; Mestdagh, H.; Simon, A.; Le Caer, S.; Ortega, J. M.; Glotin, F.; Maitre, P. *Phys. Rev. Lett.* **2002**, *89*, 273002.
(42) Prell, J. S.; O'Brien, J. T.; Williams, E. R. *J. Am. Soc. Mass Spectrom.* **2010**, *21*, 800.
(43) Lee, C.; Yang, W.; Parr, R. G. *Phys. Rev. B* **1988**, *37*, 785.
(44) Becke, A. D. *J. Chem. Phys.* **1993**, *98*, 5648.
(45) Frisch, M. J.; et al.; *Gaussian03*, Revision C.02. See Supporting Information for complete reference.
(46) Hay, P. J.; Wadt, W. R. *J. Chem. Phys.* **1985**, *82*, 270.
(47) Wadt, W. R.; Hay, P. J. *J. Chem. Phys.* **1985**, *82*, 284.
(48) Hay, P. J.; Wadt, W. R. *J. Chem. Phys.* **1985**, *82*, 299.
(49) Stevens, W. J.; Krauss, M.; Basch, H.; Jasien, P. G. *Can. J. Chem.* **1992**, *70*, 612.
(50) Franska, M.; Franski, R.; Schroeder, G.; Springer, A.; Beck, S.; Linscheid, M. *Rapid Commun. Mass Spectrom.* **2005**, *19*, 970.
(51) Hunter, E. P.; Lias, S. G. Proton Affinity Evaluation. In *NIST Chemistry WebBook*; Linstrom, P. J., Mallard, W. G., Eds.; NIST Standard Reference Database Number 69; National Institute of Standards and Technology: Gaithersburg, MD, 2005; http://webbook.nist.gov.
(52) Basch, H.; Krauss, M.; Stevens, W. J.; Cohen, D. *Inorg. Chem.* **1986**, *25*, 684.
(53) Baik, M. H.; Friesner, R. A.; Lippard, S. J. *J. Am. Chem. Soc.* **2003**, *125*, 14082.
(54) Wang, Y. S.; Chang, H. C.; Jiang, J. C.; Lin, S. H.; Lee, Y. T.; Chang, H. C. *J. Am. Chem. Soc.* **1998**, *120*, 8777.
(55) Kamariotis, A.; Boyarkin, O. V.; Mercier, S. R.; Beck, R. D.; Bush, M. F.; Williams, E. R.; Rizzo, T. R. *J. Am. Chem. Soc.* **2006**, *128*, 905.
(56) Bakker, J. M.; Sinha, R. K.; Besson, T.; Brugnara, M.; Tosi, P.; Salpin, J. Y.; Maitre, P. *J. Phys. Chem. A* **2008**, *112*, 12393.
(57) Bakker, J. M.; Salpin, J. Y.; Maitre, P. *Int. J. Mass Spectrom.* **2009**, *283*, 214.
(58) Scuderi, D.; Le Barbu-Debus, K.; Zehnacker, A. *Phys. Chem. Chem. Phys.* **2011**, *13*, 17916.
(59) Laxer, A.; Major, D. T.; Gottlieb, H. E.; Fischer, B. *J. Org. Chem.* **2001**, *66*, 5463.
(60) Seckarova, P.; Marek, R.; Malinakova, K.; Kolehmainen, E.; Hockova, D.; Hocek, M.; Sklenar, V. *Tetrahedron Lett.* **2004**, *45*, 6259.
(61) Shugar, D.; Psoda, A. In *Biophysics. Nucleic Acids. Physical Data II. Theoretical Investigations*; Saenger, W., Ed.; Springer: Berlin, 1990.
(62) Guerra, C. F.; Bickelhaupt, F. M.; Saha, S.; Wang, F. *J. Phys. Chem. A* **2006**, *110*, 4012.
(63) Rajabi, K.; Theel, K.; Gillis, E. A. L.; Beran, G.; Fridgen, T. D. *J. Phys. Chem. A* **2009**, *113*, 8099.
(64) Stearns, J. A.; Seaiby, C.; Boyarkin, O. V.; Rizzo, T. R. *Phys. Chem. Chem. Phys.* **2009**, *11*, 125.